EUMETSAT
AC SAF

AC SAF VALIDATION REPORT

NRT and Offline GOME-2C Absorbing Aerosol Index product

Authors	**Institute**
L.G. Tilstra	Royal Netherlands Meteorological Institute (KNMI)
O.N.E. Tuinder	Royal Netherlands Meteorological Institute (KNMI)
P. Stammes	Royal Netherlands Meteorological Institute (KNMI)

Document status sheet

Issue	Date	Page(s)	Modified Items / Reason for Change
1/2019	09-10-2019	all	first official version

Related products list

ID Number	Product Description
O3M-362	NRT AAI from PMDs from GOME-2C
O3M-363	Offline AAI from PMDs from GOME-2C

Contents

Introduction to EUMETSAT Satellite Application Facility on Atmospheric Composition monitoring (AC SAF)

Background

The monitoring of atmospheric chemistry is essential due to several human caused changes in the atmosphere, like global warming, loss of stratospheric ozone, increasing UV radiation, and pollution. Furthermore, the monitoring is used to react to the threads caused by the natural hazards as well as follow the effects of the international protocols.

Therefore, monitoring the chemical composition and radiation of the atmosphere is a very important duty for EUMETSAT and the target is to provide information for policy makers, scientists and general public.

Objectives

The main objectives of the AC SAF is to process, archive, validate and disseminate atmospheric composition products (O_3, NO_2, SO_2, BrO, HCHO, H_2O, OClO, CO, NH_3), aerosol products and surface ultraviolet radiation products utilising the satellites of EUMETSAT. The majority of the AC SAF products are based on data from the GOME-2 and IASI instruments onboard MetOp satellites.

Another important task besides the near real-time (NRT) and offline data dissemination is the provision of long-term, high-quality atmospheric composition products resulting from reprocessing activities.

Product categories, timeliness and dissemination

NRT products are available in less than three hours after measurement. These products are disseminated via EUMETCast, WMO GTS or internet.

- Near real-time trace gas columns (total and tropospheric O_3 and NO_2, total SO_2, total HCHO, CO) and ozone profiles
- Near real-time absorbing aerosol indexes from main science channels and polarisation measurement detectors
- Near real-time UV indexes, clear-sky and cloud-corrected

Offline products are available within two weeks after measurement and disseminated via dedicated web services at EUMETSAT and AC SAF.

- Offline trace gas columns (total and tropospheric O_3 and NO_2, total SO_2, total BrO, total HCHO, total H_2O) and ozone profiles
- Offline absorbing aerosol indexes from main science channels and polarisation measurement detectors
- Offline surface UV, daily doses and daily maximum values with several weighting functions

Data records are available after reprocessing activities from the EUMETSAT Data Centre and/or the AC SAF archives.

- Data records generated in reprocessing
- Surface Lambertian-equivalent reflectivity
- Total OClO

Users can access the AC SAF offline products and data records (free of charge) by registering at the AC SAF web site.

More information about the AC SAF project, products and services: http://acsaf.org/

AC SAF Helpdesk: helpdesk@acsaf.org

Twitter: https://twitter.com/Atmospheric_SAF

1 Introduction

1.1 Document purpose and scope

This document is the Validation Report (VR) for the NRT and offline GOME-2C Absorbing Aerosol Index (AAI) products produced at KNMI in the framework of the AC SAF (Satellite Application Facility on Atmospheric Composition Monitoring). The aim of this VR is to present the outcome of the validation study, and to report to the users the quality that they may expect.

1.2 AC SAF

The EUMETSAT Satellite Application Facility on Atmospheric Composition Monitoring (AC SAF) has been developed to provide good quality data for monitoring and research of atmospheric chemistry and composition. More specifically, the AC SAF processes, archives, validates and disseminates atmospheric data products of ozone, various trace gases such as SO_2 and NO_2, aerosols, surface reflectivity and surface ultraviolet radiation using the measurements performed by the Meteorological Operational (MetOp) satellites of EUMETSAT.

More information on the AC SAF and available data can be found on the following web page:

https://acsaf.org/

1.3 Heritage

The Absorbing Aerosol Index (AAI) was originally developed to support the Total Ozone Mapping Spectrometer (TOMS) ozone retrieval algorithm [*Herman and Celarier*, 1997; *Torres et al.*, 1998]. TOMS measurements started in 1978, and a long data record of AAI from various satellite sensors is available for studies into the impact of aerosols on climate and trace gas retrievals.

The AAI has also been developed for the European satellite sensors GOME on ERS-2 [*de Graaf et al.*, 2005] and SCIAMACHY on Envisat [*Tilstra et al.*, 2012a]. The GOME-2 AAI discussed in this validation report is the direct descendant of the SCIAMACHY AAI product.

1.4 Processor and database versions

The processor versions and database versions of the GOME-2C NRT and offline AAI products discussed in this VR are summarised in Table 1.

MetOp-C Time Period	PPF Version	PGE Version	Processing Type
2019–01–03 — 2019–02–11	6.3	2.02	NRT & Offline
2019–02–12 — 2019–07–15	6.3	2.03	NRT & Offline
2019–07–16 — 2019–10–07	6.3	2.06	NRT & Offline

Table 1: GOME-2/MetOp-C AAI: Overview of version numbers of the Product Processor Facility (PPF) and Product Generation Element (PGE) and time windows in which these were active.

1.5 Getting access to the data

Interested users can get access to the data via the EUMETSAT UMARF, the unified meteorological archive facility. The procedure involves a registration and after this step the user can select and request the data. For more information please consult the "Access to Data" section on the EUMETSAT website, or go directly to the UMARF archive via the following URL:

http://archive.eumetsat.int/umarf/

1.6 Abbreviations and acronyms

AAH	Absorbing Aerosol Height
AAI	Absorbing Aerosol Index
AC SAF	Satellite Application Facility on Atmospheric Composition Monitoring
AOT	Aerosol Optical Thickness
ATBD	Algorithm Theoretical Basis Document
BBA	Biomass Burning Aerosol
BRDF	Bidirectional Reflectance Distribution Function
BSA	Black-Sky Albedo
CDOP	Continuous Development & Operations Phase
COT	Cloud Optical Thickness
DAK	Doubling-Adding KNMI
DDA	Desert Dust Aerosols
DOAS	Differential Optical Absorption Spectroscopy
DU	Dobson Units, 2.69×10^{16} molecules cm^{-2}
ENVISAT	Environmental Satellite
EOS-Aura	Earth Observing System – Aura satellite
ERS	European Remote Sensing Satellite
ESA	European Space Agency

ETOPO-4	Topographic & Bathymetric data set from the NGDC, 4 arc-min. resolution
EUMETSAT	European Organisation for the Exploitation of Meteorological Satellites
FOV	Field-of-View
FRESCO	Fast Retrieval Scheme for Clouds from the Oxygen A band
FWHM	Full Width at Half Maximum
GMTED2010	Global Multi-resolution Terrain Elevation Data 2010
GOME	Global Ozone Monitoring Experiment
HDF	Hierarchical Data Format
IT	Integration Time
KNMI	Koninklijk Nederlands Meteorologisch Instituut
LER	Lambertian-Equivalent Reflectivity
LUT	Look-Up Table
MERIS	Medium Resolution Imaging Spectrometer
METOP	Meteorological Operational Satellite
MLS	Mid-Latitude Summer
MSC	Main Science Channel
NGDC	NOAA's National Geophysical Data Center (Boulder, Colorado, USA)
NISE	Near-real-time Ice and Snow Extent
NOAA	National Oceanic and Atmospheric Administration
NRT	Near-Real-Time
OMI	Ozone Monitoring Instrument
O3M SAF	Satellite Application Facility on Ozone and Atmospheric Chemistry Monitoring
PMD	Polarisation Measurement Device
PSD	Product Specification Document
PUM	Product User Manual
RMSE	Root-Mean-Square Error
RTM	Radiative Transfer Model
SCIAMACHY	Scanning Imaging Absorption Spectrometer for Atmospheric Chartography
SZA	Solar Zenith Angle
TEMIS	Tropospheric Emission Monitoring Internet Service
TOA	Top-of-Atmosphere
TOMS	Total Ozone Mapping Spectrometer
UTC	Universal Time Co-ordinate
UV	Ultraviolet
VIS	Visible
VR	Validation Report
VZA	Viewing Zenith Angle

2 Instrument degradation

The degradation correction for the GOME-2C AAI is not applied yet, because a full year of data is needed to be able to separate the effects of instrument degradation from the normal seasonal cycle seen in the global mean reflectance. The degradation monitoring for the GOME-2C AAI is operational. Currently, the impact of degradation correction on the GOME-2C AAI is low.

2.1 Introduction

Instrument degradation is a serious problem which strongly affects the Earth reflectance measurements performed by GOME-2 in the UV wavelength range [*Tilstra et al.*, 2012b]. As a result, it also has an impact on the AAI products retrieved from the GOME-2 instruments [*Tilstra et al.*, 2010]. For this reason, we apply correction factors to the Earth reflectances that are found in the GOME-2 level-1b product. The method that we use to derive these in-flight degradation correction factors has been introduced earlier in *Tilstra et al.* [2012a] for the SCIAMACHY instrument. The method was later successfully applied to correct the GOME-2 instruments [*Tilstra et al.*, 2012b].

2.2 Measuring instrument degradation

The method is based on studying time series of the daily global mean reflectance. The daily global mean reflectance, denoted by $R^{\star}$, is defined as the mean of all measured Earth reflectances for a certain scan mirror position on a certain day between 60°N and 60°S and solar zenith angles θ_0 less than 85 degrees. In Figure 1 we present two plots as done in *Tilstra et al.* [2012b] which show the daily global mean reflectance as a function of time for the GOME-2A instrument.

The time series of the global mean reflectance show seasonal variations as well as trends due to instrument degradation. To analyse the time series, we assume that the global mean reflectance may be well described empirically by a function made up of a polynomial term, representing the reflectance change due to instrument degradation, multiplied by a term periodic in time that represents the normal seasonal variation of the global mean reflectance. In other words,

$$R^{\star}_{\lambda,s} = P^{(p)}_{\lambda,s} \cdot \left[1 + F^{(q)}_{\lambda,s}\right], \tag{1}$$

where the term P represents the polynomial part of degree p, defined by

$$P^{(p)}_{\lambda,s}(t) = \sum_{m=0}^{p} u^{(m)}_{\lambda,s} \cdot t^m, \tag{2}$$

while the seasonal variation F is described by a finite Fourier series of order q, according to

$$F_{\lambda,s}^{(q)}(t) = \sum_{n=1}^{q} \left[v_{\lambda,s}^{(n)} \cdot \cos(2\pi nt) + w_{\lambda,s}^{(n)} \cdot \sin(2\pi nt) \right] . \tag{3}$$

In these equations, the parameter t is the time expressed in years since the beginning of the time series (which is 4 January 2007 in the case of GOME-2 on MetOp-A). The parameter λ refers to the wavelength and the integer s relates to the scan mirror position. For GOME-2, this integer runs from 1 to 32 for the nominal integration time (IT) of 187.5 ms when the instrument scans from east to west and back. For the present baseline, we use $p = 4$ and $q = 6$ for GOME-2 on MetOp-A.
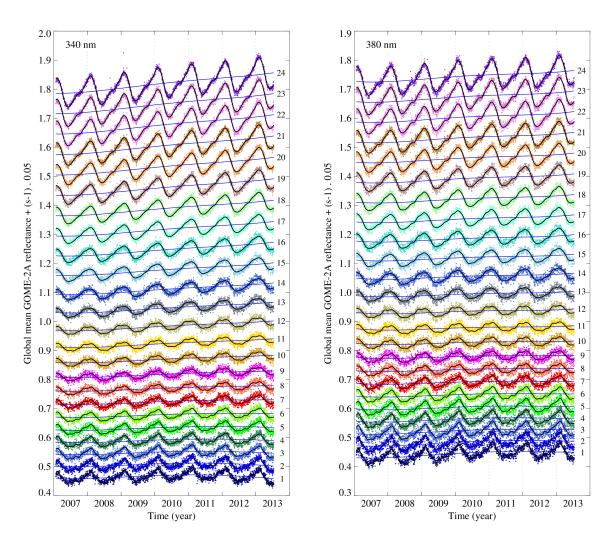

Figure 1: *Global mean reflectance measured by GOME-2A at 340 nm (left) and 380 nm (right) as a function of time, for each of the 24 scan mirror positions in the forward scan. To separate the time series graphically, an offset of $(s-1) \cdot 0.05$ was added to each, where s is the scan mirror position as indicated. The solid black curves are fit results and are described in the main text. The blue monotonous curves illustrate the effect of instrument degradation over the years.*

The polynomial part P is the most important as it represents the relative change in the GOME-2 measured Earth reflectance over the years, per scan mirror position, due to instrument degradation. Normalisation of P immediately leads to the reflectance degradation factor:

$$d_{\lambda,s}(t) = P_{\lambda,s}^{(p)}(t) \,/\, P_{\lambda,s}^{(p)}(0) \,. \tag{4}$$

For GOME-2 the reflectance degradation factor is growing with time for most wavelengths, and it is strongly dependent on scan mirror position. Figure 1 shows the behaviour for 340 and 380 nm.

2.3   Correcting instrument degradation

The correction for instrument degradation can easily be calculated using

$$c_{\lambda,s}(t) \equiv 1/d_{\lambda,s}(t) = P_{\lambda,s}^{(p)}(0) \,/\, P_{\lambda,s}^{(p)}(t) \,. \tag{5}$$

The measured Earth reflectances have to be multiplied with these correction factors. In the operational processing chain, these correction factors are determined daily, by calculating the global mean reflectances at 340 and 380 nm for the previous day, and appending the result to the historical archive of global mean reflectances. After that, the method outlined in section 2.2 is executed, which provides a forecast for the present day. Each day this procedure is repeated, yielding up-to-date full mission correction factors. The results can be monitored via the following URL:

http://www.temis.nl/acsaf/globalmean.php

The time series of global mean reflectance and corrections factors have to be calculated for each instrument, and for main science channel and PMD bands separately.

2.4   Impact of instrument degradation on the AAI

As an example of the impact of instrument degradation, we present in Figure 2 time series of the GOME-2/MetOp-A *uncorrected* global mean residue/AAI as a function of time, for each of the 24 scan mirror positions in the forward scan of the GOME-2A instrument. The *uncorrected* AAI is available in the AAI product under field name "UncorrectedResidue". Note that these data should never be used. They are available in the product for the purpose of being able to monitor the impact of instrument degradation on the (uncorrected) AAI. The *corrected* AAI data are stored under field name "AAI". These are the AAI data to be used by the users of the AAI products, and these are the AAI data that will be discussed in the remaining part of this validation report.

As can be concluded from Figure 2, the impact of instrument degradation on the AAI is indeed very large. The instrument degradation is depending on the scan mirror position. For instance, at the nadir
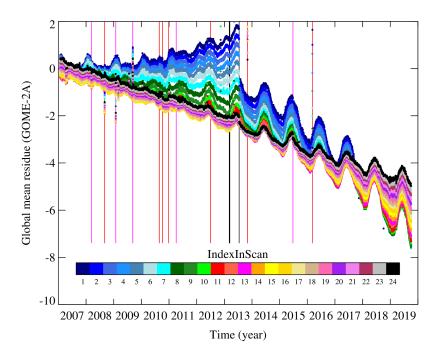
Figure 2: Daily global mean residue observed by GOME-2 on MetOp-A versus the time for all 24 forward scan mirror positions inside the GOME-2 swath. The colour bar links the colours to the "IndexInScan" number. The trend due to instrument degradation varies with scanner angle.
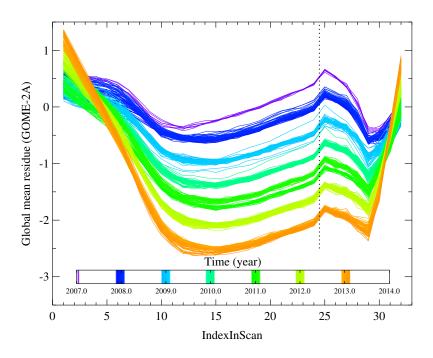

Figure 3: Global mean residue as a function of scanner mirror position, for all available days in the months December and January of the years up to 2013. The colours can be related to the actual date using the colour bar. The vertical dotted line illustrates the westernmost scanner angle position.

position in the orbit swath (IndexInScan = 12/13), the uncorrected global mean residue is currently almost 6 index points lower than at the start of the GOME-2A mission.

Several vertical lines in Figure 2 indicate notable events in the MetOp-A life time. Jumps in the global mean residue can occur at the dates associated with these lines. One vertical line corresponds to 11 March 2008. On this day, a new PMD band definition (v3.1) was uploaded to the satellite instrument. As a result, the global mean residue jumped up by ∼0.2 index points. Another vertical line corresponds to 9 September 2009, right in the middle of a throughput test of the GOME-2 instrument. The direct effect of this throughput test was very small. A third vertical line corresponds to the swath width reduction that took place on 15 July 2013. Other vertical lines are related to changes in the (level-1) processor. These events are all not related to instrument degradation and are therefore not affected, corrected or treated in any way by the algorithm.

In Figure 3 we present the same data but in a different way. We plot the dependence of the global mean residue on scanner angle for all days in the months December and January. The figure clearly demonstrates the dependence of the global mean residue on the scan mirror angle (i.e., on the scattering geometry), and the change in this dependence due to the impact of instrument degradation.

2.5   Accuracy

The correction method that we use was estimated to be accurate within 0.2% [*Tilstra et al.*, 2012a]. A trend in the Earth reflectance can therefore be removed to well within the percent level. Using the rule of thumb that a one percent change in reflectance leads to a residue change of half an index point [*Tilstra et al.*, 2012a], we estimate that the accuracy of the correction for instrument degradation is better than 0.2 index points over the entire time range covered by the GOME-2 instruments.

3 AAI products from MetOp-C

3.1 Time series of global mean AAI

Analysing the global mean residue is a simple and robust validation technique for the AAI [see, for instance, *de Graaf et al.*, 2005; *Tilstra et al.*, 2010, 2012a]. The daily global mean residue, in this report, is defined as the average of all healthy residue measurements on a day located between 60°N and 60°S and having solar zenith angles below 85 degrees. This global mean turns out to be a rather stable and predictable property, which is something we can use to validate the residue/AAI.

3.2 AAI from the Main Science Channels

In this section we present results for the global mean AAI derived from the main science channels (MSC) for individual positions of the scanner mirror. For the MSC-AAI products the reflectances are determined from two wavelength bands in spectral channel 2 (centred at 340 and 380 nm). The size of the MSC measurement footprints amounts to roughly 80×40 km^2 for the largest part of the orbit. The associated integration time (IT) is 187.5 ms for observations between 60°N and 60°S, leading to 32 measurements per scan, of which the last 8 are backscan measurements. Despite the fact that the number of measurements over which is averaged decreases by a factor of 32 (or 24) when we restrict ourselves to individual scanner mirror positions, we still end up with a statistical property which is stable enough for the time series analyses we will be performing in the rest of this section.

3.2.1 Time series

In Figure 4 we present the GOME-2/MetOp-C daily global mean MSC residue versus time for all forward scan mirror positions. There are 24 measurements inside each forward GOME-2 scan, resulting in 24 time series, each with their own colour and labelled by their own "IndexInScan" number. From Figure 4 it is immediately clear that there are no major issues. Given the experience with the GOME-2A and GOME-2B AAI products, we know that there must be some impact of instrument degradation. This impact is hard to find in Figure 4 because most of the temporal behaviour of the global means is related to the normal seasonal cycle of the AAI.

The global mean residue values in Figure 4 are mostly found between 0 and 1 index point, depending on the "IndexInScan" number. For GOME-2A the global mean residues were found between -0.5 and +0.5 index points, and for GOME-2B the global mean residues were between -0.25 and +0.75 [*Tilstra et al.*, 2016]. Also compare with Figure 2. It therefore seems likely that there is a 0.25–0.5 index points offset present in the GOME-2C MSC-AAI. A most likely explanation for this is a (very
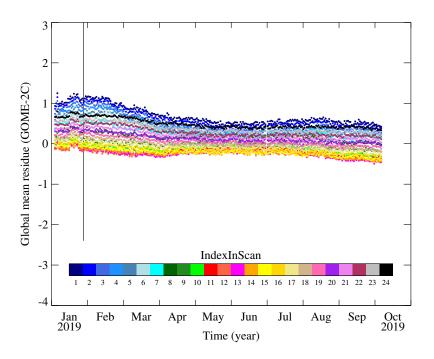
Figure 4: Daily global mean residue from the main science channels for all 24 forward scan mirror positions inside the GOME-2C swath plotted versus the time. The colours relate to the "IndexInScan" number, as indicated by the colour bar.
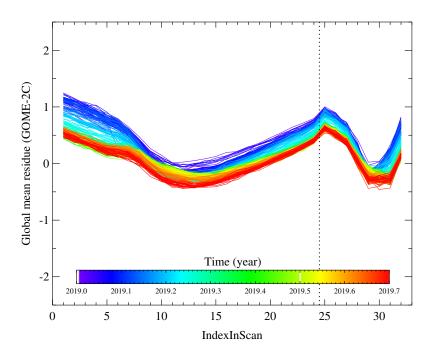

Figure 5: Global mean residue from the main science channels as a function of scanner mirror position. The colours can be related to the actual date using the colour bar. The vertical dotted line illustrates the westernmost scanner angle position.

small) error in the radiometric calibration of the GOME-2C instrument.

The vertical line plotted in Figure 4 indicates the end of the commissioning phase of GOME-2C. The commissioning phase ended on 28/29 January 2019. No jumps or other features can be seen in the time series around this date. However, before this date there is a short time period with slightly higher (+0.1 index point) global mean residues. Given that this is only a very small offset, we conclude that the MSC-AAI data from the commissioning phase can safely be used.

In Figure 5 we present the global mean residue as a function of scanner mirror position, for all available days. The colours can be related to the actual date using the colour bar. Note that the global mean AAI of the backscan pixels is displayed also. The vertical dotted line indicates the turning point of the motion of the scan mirror at the west side of the orbit swath. Figure 5 should be compared to Figure 3, or to figures 20 and 30 presented in *Tilstra et al.* [2016]. When making these comparisons, one should compare data from the same time of the year (to avoid difference due to the seasonal cycle of the global mean AAI). Also, note that for the data in Figure 3 the degradation correction was not applied. This is not a problem for figures 20 and 30 presented in *Tilstra et al.* [2016].

From the comparisons we conclude that compared to the GOME-2A MSC-AAI, the GOME-2C MSC-AAI has an offset of +0.25 for the west and nadir part of the orbits swath, but a +0.5 index points offset at the east side of the orbit swath. Compared to the GOME-2B MSC-AAI, the GOME-2C MSC-AAI has an offset of +0.25 for the west part of the orbits swath, a near zero offset for the nadir part, but a +0.5 index points offset at the east side of the orbit swath. Although these differences are relatively small, they do point to a scan-angle dependent offset, which makes it more complicated to derive an (accurate) correction for the differences.

3.3   AAI from the PMD bands

The AAI products derived from polarisation measurement device (PMD) band measurements are derived from reflectances measured by PMD-p bands 5 and 7, currently configured to wavelengths of 338 and 382 nm. The main advantage of the PMD-AAI product compared to the MSC-AAI product is the smaller footprint size, which amounts to roughly 10×40 km^2. For the validation of the PMD-AAI we follow basically the same procedure as for the MSC-AAI.

3.3.1   Time series

In Figure 6 we present time series of the global mean residue determined from PMD band measurements by GOME-2 onboard MetOp-C. Only a fraction of the 192 PMD scan mirror positions of the forward scan are shown (see colour bar). Data from before 28 January 2019 (indicated by the vertical
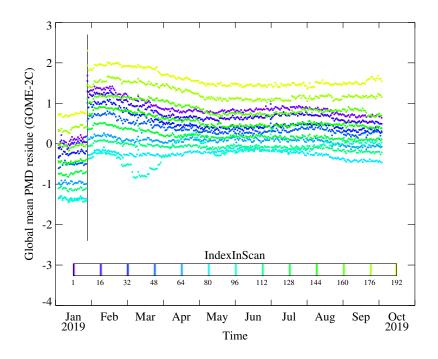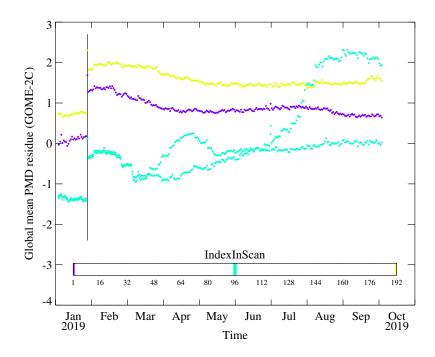
Figure 6: Daily global mean residue versus time for a selection of the 192 forward scan PMD scan mirror positions inside the GOME-2C orbit swath. The colours relate to the "IndexInScan" number, as indicated by the colour bar. Notice the jump at the end of the commissioning phase (28 January 2019), indicated by the vertical line. The residue jumps up by ~one index point after this date.

Figure 7: Similar to Figure 6 but now only the centre and extreme scan mirror positions are plotted. Notice the very different behaviour of IndexInScan 96 and 97.

line) are plotted although these are data from the commissioning phase. The residues calculated from data from the commissioning phase are lower by on average one index point than the residues after 28 January 2019. The reason for this jump is related to changes in key data. Apparently this affected mostly the PMD bands, and not so much the main science channels (also see Figure 4).

Comparing Figure 6 with figures 25 and 33 presented in *Tilstra et al.* [2016] we find that before the end of the commissioning phase (28 January 2019) the GOME-2C PMD-AAI is too low by -0.25 index points. After the end of the commissioning phase, however, the GOME-2C PMD-AAI is too high by almost one index point. Also compared to the MSC-AAI it is clear that there is a relatively large offset of about one index point present in the GOME-2C PMD-AAI. In Figure 7 we present a plot similar to Figure 6, but now for the extreme scan mirror positions (IndexInScan=1,192) and for nadir (IndexInScan=96,97). The temporal behaviour of IndexInScan 96 and 97 should be similar but they are very different and both show strange temporal behaviour.

In Figure 8 we present the same global mean PMD residue, but now as a function of scan mirror position. Backscan measurements are also shown, the scan mirror position therefore runs from 1 to 256. The vertical dotted line indicates the turning point, where the scan mirror changes direction of movement. Note that the retrieval at scan mirror positions 240–244 fails. Pixels 240–243 are known as reset pixels [*Munro and Lang*, 2011], and do not produce valid measurements. Pixel 244, next in line after the reset pixels, produces radiances which are not to be trusted. Note that these measurements are performed during the backscan of the instrument. Also note that the backscan pixels show the same behaviour as the forward scan pixels, taking into account that the scanning direction is reversed and that the scan speed is three times as high.

Comparing Figure 8 with figures 26 and 34 presented in *Tilstra et al.* [2016] we find a number of differences. First of all, the global mean residues from the GOME-2A and GOME-2B PMD-AAI were more or less symmetric in shape from east to west. This is not the case for the GOME-2C PMD-AAI, which shows an offset of +0.5 index points on the west side of the orbit swath with respect to the east side of the orbit swath. Secondly, in general the values of the GOME-2C PMD-AAI are higher by 0.4–0.8 index points. Thirdly, a feature shows up around "IndexInScan" position between 94–98 in the form of a "spike".

To study this "spike" more closely, Figure 9 zooms in on the "IndexInScan" range between 91 and 101. The "spike" is not confined to one IndexInScan position. Instead, it seems to be a feature that exists between IndexInScan range 94–98. The feature started to appear somewhere in February 2019. It seems to grow with time although it also seems to become less wide. It is not understood where this feature is coming from. In the GOME-2A and GOME-2B PMD-AAI such a feature was not found, yet revisiting figures 26 and 34 presented in *Tilstra et al.* [2016] and looking more closely to the figures we do indeed find similar (but small) features for the same scanner mirror positions. Whatever the features are, they are only found in the PMD-AAI. The fact that the feature is growing
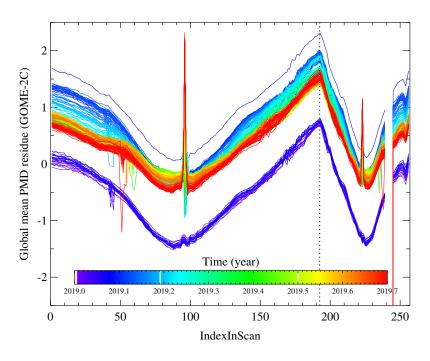
Figure 8: Global mean PMD residue measured by GOME-2C on the as a function of scanner mirror position. Compare with Figure 5. The spikes occurring near "IndexInScan" numbers 94–98 are studied more closely in Figure 9.
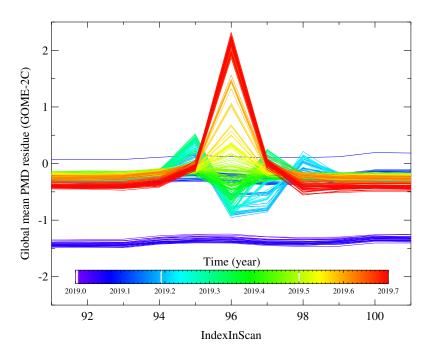

Figure 9: Global mean PMD residue measured by GOME-2C on the as a function of scanner mirror position for IndexInScan range 91–101. The spikey behaviour within IndexInScan range 94–98 is not understood.

suggests a growing imperfection in the polarisation retrieval for the scanner mirror positions 94–98. However, this is, at this point, speculation.

3.3.2   Images

The main advantage of the PMD-AAI over the MSC-AAI is the higher spatial resolution. The footprint size amounts to roughly $10 \times 40 \, \mathrm{km}^2$. In Figures 10 we present a global image of the PMD-AAI. The case (of 20 May 2019) is that of smoke from Canadian forest firest. The smoke plume is captured extremely well by the PMD-AAI in subsequent orbits. Figure 11 present the AAI from the TROPOMI instrument for the same day, for comparison. The TROPOMI AAI seems to be too low, this is a known problem. Otherwise, the agreement is rather good.

A second case (of 11 September 2019) is shown in Figures 12 and 13. This is a case of biomass burning smoke originating from South America flowing over the South Atlantic ocean. Again the agreement is very good, apart from the difference in magnitude of the AAI. The high spatial resolution of the PMD-AAI makes it ideally suited for monitoring aerosol plumes. Notice that the "spikes" that were found near "IndexInScan" manifest themselves as reddish tracks along the orbits in Figure 12. The feature seems to become stronger near the poles, where the degree of polarisation is, generally speaking, the highest. This suggests that the polarisation retrieval is making errors calculating the PMD radiances and polarisation. The fact that earlier data do not show the feature would point to the time-dependent adjustments that are made to the polarisation key data.
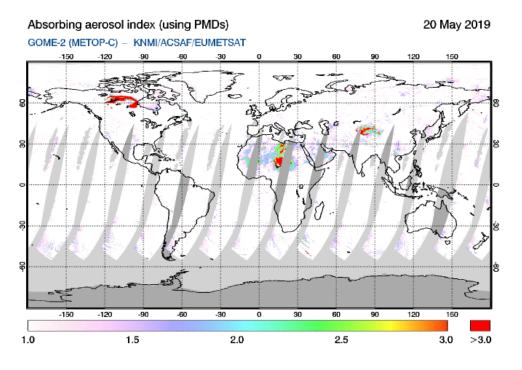
Figure 10: Global map of the PMD-AAI measured by GOME-2 on MetOp-C for 20 May 2019.
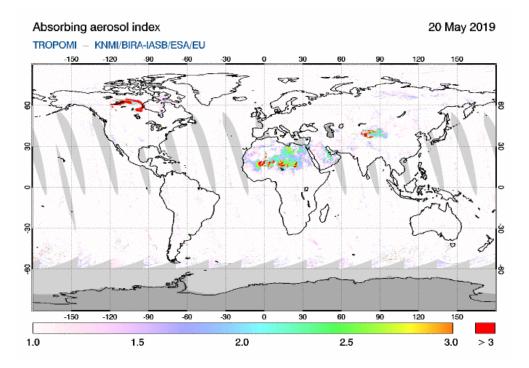

Figure 11: Global map of the AAI measured by TROPOMI on Sentinel-5P for 20 May 2019.
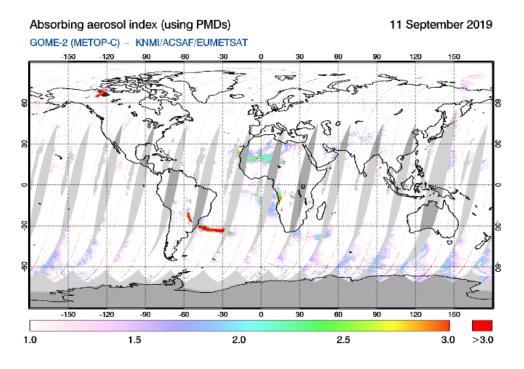
Figure 12: Global map of the PMD-AAI measured by GOME-2 on MetOp-C for 11 September 2019.
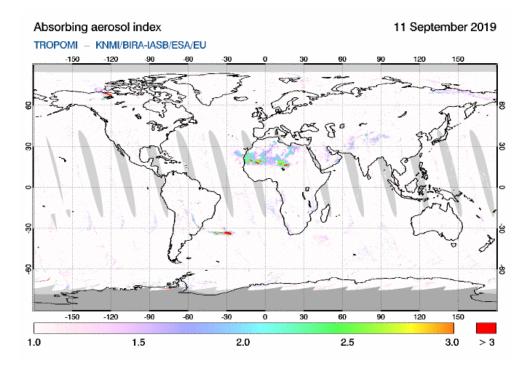

Figure 13: Global map of the AAI measured by TROPOMI on Sentinel-5P for 11 September 2019.

4　Summary and conclusions

The MSC-AAI from MetOp-C seems to be in a good shape. The analyses of the global mean AAI indicate that there is a good agreement with the GOME-2A and GOME-2B MSC-AAI products. Compared to these two products, there seems to be a small offset present in the GOME-2C MSC-AAI of 0.25–0.5 index points. The MSC-AAI data from the commissioning phase are not of a lesser quality than those from after the commissioning phase and can therefore be used safely.

For the PMD-AAI we find different behaviour. First of all, the data from the commissioning phase are systematically lower. Time series of the global mean PMD-AAI show that there is a jump of about one index point at the end of the commissioning phase. Compared to the GOME-2A and GOME-2B PMD-AAI products the GOME-2C PMD-AAI appears to be, on average, too high by 0.4–0.8 index point, depending on the scanner mirror position. A weird feature, described earlier as a "spike" for lack of a better word, appears in the time series and in global images around February 2019. The feature seems to become stronger with time and is clearly visible in the global images. The cause of the feature is not yet clear, but it seems likely that it is caused by issues in the polarisation retrieval.

References

de Graaf, M., P. Stammes, O. Torres, and R. B. A. Koelemeijer (2005), Absorbing Aerosol Index: Sensitivity analysis, application to GOME and comparison with TOMS, *J. Geophys. Res., 110*, D01201, doi:10.1029/2004JD005178.

EUMETSAT (2014), GOME-2 Factsheet, Doc. No. EUM/OPS/DOC/10/1299, Issue 4a, 20 May 2014, EUMETSAT, Darmstadt, Germany.

Herman, J. R., and E. A. Celarier (1997), Earth surface reflectivity climatology at 340–380 nm from TOMS data, *J. Geophys. Res., 102*(D23), 28,003–28,011, doi:10.1029/97JD02074.

Munro, R. and R. Lang (2011), GOME-2 Level 1 Product Generation Specification, Doc. No. EPS.SYS.SPE.990011, Issue 7.0, 28 February, EUMETSAT, Darmstadt, Germany.

Tilstra, L. G., M. de Graaf, I. Aben, and P. Stammes (2012a), In-flight degradation correction of SCIAMACHY UV reflectances and Absorbing Aerosol Index, *J. Geophys. Res., 117*, D06209, doi:10.1029/2011JD016957.

Tilstra, L. G., O. N. E. Tuinder, and P. Stammes (2010), GOME-2 Absorbing Aerosol Index: statistical analysis, comparison to GOME-1 and impact of instrument degradation, in *Proceedings of the 2010 EUMETSAT Meteorological Satellite Conference*, EUMETSAT P.57, ISBN 978-92-9110-089-7, Cordoba, Spain.

Tilstra, L. G., O. N. E. Tuinder, and P. Stammes (2012b), Introducing a new method for in-flight degradation correction of the Earth reflectance measured by GOME-2, and application to the AAI, in *Proceedings of the 2012 EUMETSAT Meteorological Satellite Conference*, EUMETSAT P.61, Sopot, Poland.

Tilstra, L. G., O. N. E. Tuinder, and P. Stammes (2016), Reprocessed GOME-2 Absorbing Aerosol Index product – Validation Report, *KNMI Report SAF/O3M/KNMI/ATBD/003*, Issue 2/2016, March 1, 2016.

Torres, O., P. K. Bhartia, J. R. Herman, Z. Ahmad, and J. Gleason (1998), Derivation of aerosol properties from satellite measurements of backscattered ultraviolet radiation: Theoretical basis, *J. Geophys. Res., 103*(D14), 17,099–17,110, doi:10.1029/98JD00900.